Reduction of atmospheric disturbances in PSInSAR measure technique based on ENVISAT ASAR data for Erta Ale Ridge

Anna Kopeć[1,*]

[1]Wroclaw University of Science and Technology, Faculty of Geoengineering, Mining and Geology, 27 Wyb. Wyspianskiego St., 50-370 Wroclaw, Poland

Abstract. The interferometric synthetic aperture radar (InSAR) is becoming more and more popular to investigate surface deformation, associated with volcanism, earthquakes, landslides, and post-mining surface subsidence. The measuring accuracy depends on many factors: surface, time and geometric decorrelation, orbit errors, however the largest challenges are the tropospheric delays. The spatial and temporal variations in temperature, pressure, and relative humidity are responsible for tropospheric delays. So far, many methods have been developed, but researchers are still searching for the one, that will allow to correct interferograms consistently in different regions and times. The article focuses on examining the methods based on empirical phase-based methods, spectrometer measurements and weather model. These methods were applied to the ENVISAT ASAR data for the Erta Ale Ridge in the Afar Depression, East Africa

1 Introduction

The Interferometric Synthetic Aperture Radar (InSAR), is a modern technique for measuring the deformation of the Earth's surface, using electromagnetic waves emitted by instruments installed on satellites. The electromagnetic wave, covering twice the distance between the satellite, and the measuring object, is exposed to the effects of various external factors. One of them is the Earth's atmosphere. Currently, the reduction of impact of the atmosphere, is one of the biggest challenges for measurements with the InSAR techniques.

2 The research object (Erta Ale Ridge)

The volcanic ridge Erta Ale, is situated in the area of the Afar Depression, in Eastern Africa, at the junction of the three tectonic plates: Nubian (African), Arabic, and Somali. This is an

* Corresponding author: anna.kopec@pwr.edu.pl

area of active continental rift, the northern fragment of East African Rift (Fig. 1). In the area of Afar, the Arab and Somali Plates move away from the stable Nubian Plate [1]. The Erta Ale region is of shield volcano nature, which is characteristic of the continental rift, still there lie also stratovolcanoes. The volcanic chambers occur very shallowly beneath the surface of the Earth (< 2 km). In the very crater of Erta Ale, there is an exposed lava lake [2]. Eruptions, closely related to the seismic shocks, can cause considerable dislocations, both in the vertical and in the horizontal plane [3].

The important object in the region of the Erta Ale Massif is the volcanic group Alu Dallafila, situated 30 km south of the main crater of Erta Ale. Alu - Dallafila is made up of basalt volcanic cone - Alu, stratovolcano- Dalafilla and basalt volcanic area Alu South lying between them (Fig. 1). Until 2008, only fumarolic activity was observed. On November 3rd, 2008 the eruption began, which started with the earthquake. The eruption was associated with significant displacement of the terrain, reaching the value of up to 1.9 m for the Alu cone and about 1 m in the Alu South region [3]. Today, it is the only one observed eruption of this area in the Erta Ale region.

The Afar Depression Area, due to the lack of vegetation and the prevalence of desert areas, volcanic covers and saltwater lakes, allows for very large numbers of Pernament Scatter (PS) points.

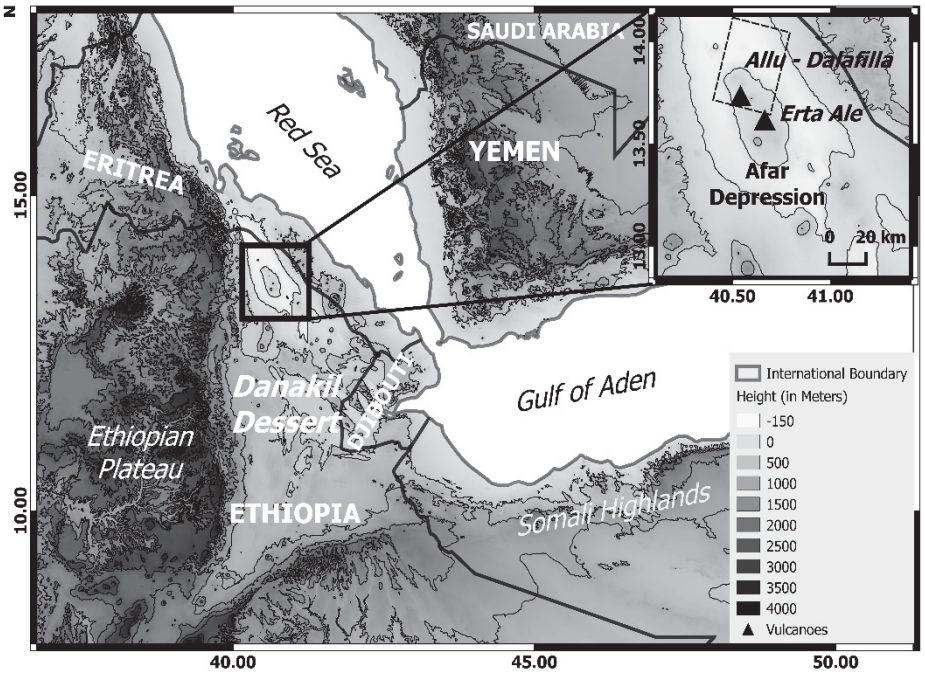

Fig. 1. The research object Erta Ale Ridge – dashed polygon indicate the ground area of InSAR data.

3 PSInSAR measurements

The calculations used 45 ENVISAT-ASAR satellite imaginery, from path 049, taken in the period since November 28th, 2003 to September 17th, 2010. The imagery area includes the northern part of the Erta Ale Massif - including Alu - Dallafila volcanoes, measuring approximately 29 x 38 km and the area of approximately 1 100 km^2. The data cover the period before and after the earthquake in November 2008. The interferograms were created using

the Delft Object-oriented Radar Interferometric Software (DORIS) [4]. PSInSAR processing was performed in Stanford Method for Persistent Scatterers (StaMPS) software [5]. A total of 205,793 PS points were identified, characterized by a large and stable wave reflection time. All interferograms refer to the master image taken on November 21st, 2008, so the significant land displacements, due to earthquakes and eruptions of November 3rd, 2008, would be visible to images taken prior to the master image. The results obtained, confirm the previous research carried out by Pagli [3]. In the area of the Alu cone, the terrain was reduced by more than 1 m (Fig. 2).

It should be noted, that the calculation results, for both the displacements and the delays are set in radians, formula (1) should be applied to change the unit to centimeters.

$$\Delta\phi_{cm} = \frac{\lambda \cdot \Delta\phi}{4\pi} \tag{1}$$

where:
ϕ_{cm} – phase change in centimeters,
λ – the radar wavelenth,
$\Delta\phi$ – phase change in radians.

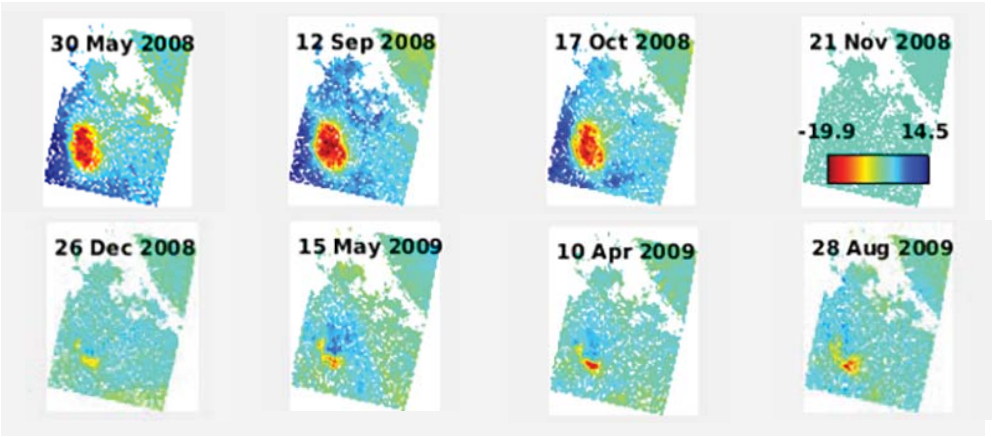

Fig. 2. Unwraped phase reduced by DEM and orbits errors for selected images, values are set in radians.

4 Atmospheric delay in the InSAR measurements

The inhomogeneity of the atmosphere (the ionosphere and the troposphere) and its variability in time and space, cause change in the signal speed on the geometrical path between the antenna and the surface of the terrain. It has been observed in the 1990's that this may create problems in the interpretation of interferograms [6]. The atmospheric delay is also referred to as an atmospheric signal, or an atmospheric phase screen (APS). Measurement errors, resulting in atmospheric delay, can range up to ± 15 - 20 cm [7], which can have a significant impact on the identification and interpretation of deformation. Conditions in the troposphere and the ionosphere have the greatest impact on the signal course. Due to the differential nature of the InSAR technique measurements, the difference between two interferogram images, creating the given interferogram, is more significant than the value of the atmospheric delay.

In the ionosphere, the course of an electromagnetic wave is disturbed by changes in the Total Electron Content (TEC) along with its propagation path. Because of the greater width and dispersion nature of the phenomenon, the ionospheric refraction has a much greater effect

on the propagation of longer waves ranging from P and L. Signal disturbances for C waves are minimal and do not affect the InSAR measurements [8].

In the case of C waves, atmospheric delay is often referred to as a tropospheric delay because it is caused by tropospheric refraction. In the troposphere there is a high spatial variability of such factors as temperature, pressure, and relative air humidity. The tropospheric refraction can be divided into two components: the dry hydrostatic (N_{hydr}) and the wet hydrostatic (N_{wet}). The tropospheric delay for the signal phase is determined by the change of the two refraction components along the geometrical path between the antenna and the terrain surface (2).

$$\phi_{tropo} = \frac{-4\pi}{\lambda}\frac{10^{-6}}{cos\theta}\int_{h}^{h_{top}}(N_{hydr} + N_{wet})dx \quad (2)$$

where:
θ - the incidence angle.

4.1 The wet component of the tropospheric refraction

The wet component of the tropospheric delay depends on the distribution of relative air humidity, which changes dynamically, both in the vertical and horizontal plane. These changes are turbulent and result in many factors, including: thermal convection, differences in direction and speed of wind at different altitudes, friction, and extensive weather systems. The delay resulting from these disturbances is very difficult to model [7, 9].

4.2 The dry component of the tropospheric refraction

The dry component of the tropospheric delay is represented by the vertical temperature distribution and dry air pressure. The troposphere is divided into an infinite number of layers characterized by various refraction values, and their vertical span is variable over time. This is important for the terrains with large areas of height differences [9].

5 Determination and reduction of delay

Different approaches are used to determine the tropospheric delay in InSAR techniques and additional data from: spectrometers [7, 10], weather models [7, 11], GNSS measurements [12] are used. However, data from different sources are characterized by different temporal and spatial resolution in relation to the interferometric data. The approach based on determining delay in an empirical way, directly from the interferograms [7, 13] is also applied. In this paper, delay has been determined by means of three methods: the spectrometric, empirical (linear), and based on weather data models.

5.1 Empirical method - linear

Tropospheric delay, empirically designated directly from interferograms, is specified by the linear relationship between the phase and topography (3) [13].

$$\Delta\phi_{tropo} = K_{\Delta\phi}h + \Delta\phi_0 \quad (3)$$

where:
$K_{\Delta\phi}$ is the estimate of the top-phases relation,
h - ground level,
$\Delta\phi_0$ – constant coefficient of deviation from the entire inerferogram.

Determining the delay is not differentiated into wet and dry refraction component, this is the total relative delay between the *master* and the *slave* image.

The phase-based and topography-based methods are not effective in the areas where there is no large height difference and errors are mainly due to seasonal and local atmospheric variability.

5.2 The spectrometric method

The spectrometric data allow to measure the total amount of Precipitable Water Vapor (PWV). The PWV is determined by the ratio of radiation absorbed on the channel sensitive and insensitive to the presence of water vapor in the air [14]. Based on the PWV, a Zenith Wet Delay (ZWD) can be determined - formula 4, followed by wet tropospheric delay formula 5 [14],

$$ZWD = \Pi \cdot \mathrm{PWV} \tag{4}$$

where Π is the PWV transformation coefficient for zenithal delay. Π usually takes on the value of about 6.2.

$$\phi_{tropo}^{wet} = \frac{-4\pi}{\lambda}\frac{ZWD}{cos\theta} \tag{5}$$

The spectrometric data allow to determine only the wet delay component that is associated with turbulent tropospheric disorders. Spectrometers are passive sensors that perform measurements exclusively in daytime and under clear conditions. The calculations used data from the MERIS spectrometer, which operated on the ENVISAT platform. This avoids errors associated with temporal and spatial interpolation.

5.3 The ERA-I weather model

Weather models are generated based on the surface and satellite data, providing information on pressure, temperature and relative air humidity. They allow both, wet and dry refraction to be determined. ZWD is determined in the same way as for spectrometric measurements - formulas 4 & 5. The Zenith Hydrostatic Delay (ZHD) is calculated on the basis of the Saastamoinen model [15] - formula 6, where the hydrostatic delay is determined by the relation between the latitude (φ), the height (h) and the atmospheric pressure (P).

$$ZHD = 0.0022768\frac{P}{1-0.00266cos2\varphi-0.00028h} \tag{6}$$

The ERA-I model of the resolution of about 80 km was used at the calculations. The temperature and relative humidity values are determined for 37 levels with a certain atmospheric pressure. The data acquisition interval is 6 hours. Because of the low temporal and spatial resolution, the data require interpolation.

6 Results

The reduction of delay was based on the three above described methods. It has been proven which of these methods provides the best results for the data, which illustrate a significant, rapid land displacement. The methods were compared in qualitative and quantitative terms. Qualitatively, by the data accessibility, comparing the spatial distribution of delays with terrain topography. Quantitatively, by comparing the numerical values of delays and their Root Mean Square Error (RMSE), calculated with respect to wet-field spectrometry and weather model for dry components.

The results of the empirical delay calculation by the linear method show a strong dependence on the displacement values. The delay takes on the values even up to -22 rad (about 100 cm), only for the images taken before the earthquake. The spatial location of the

delay coincides also with the location of the land displacement. For other interferograms, the delay is not varied (Fig. 3a).

The spectrometric method allowed for the determination of delay for 30 out of 44 interferograms. This was due to the lack of data availability for some images - the measurement was taken under unclear conditions, or at night. It has been assumed that the state of the sky should not exceed 20%. The calculated wet component of the delay reaches values up to approx. ± 20 rad (approximately ± 90 cm). However, the most of the values oscillate around a few radians. The delay is not explicitly correlated with topography. For several images, such as of May 30th and September 12th, 2008, and April 10th, June 19th and October 2nd, 2009, the clear limit of variation of delay in the Allu-Dallafila Massif can be seen (Fig. 3b).

The results of calculations based on data of the ERA-I weather model show the smallest delay values. For the hydrostatic component, the maximum is approx. ± 0.1 rad (approx. ± 0.4 cm) while for the wet component is approx. ± 3 rad (approx. ± 13 cm). It can be seen for the most interferograms, that the values are interpolated (Fig. 3c, d). This is due to the fact, that the resolution of the model is only 80 km, which is not enough for such a small area (29 x 38 km).

It has been verified to what extent the delays determined by the linear method and based on the weather model, for the both components, depart from the delay results of the spectrometric method combined with the dry component of the weather model. The results are presented in Table 1 and, testify to the considerable variation of linear method with respect to the spectrometric method and the weather model. RMSE for the linear method is 0.63 cm larger, compared to the weather model.

Table 1. RMSE comparison of investigation methods.

Reference - spectrometric method combined with the dry component of the weather model	Empirical linear method	Weather model (both components)
RMS	RMSE	
2.02 *cm*	2.65 *cm*	2.02 *cm*

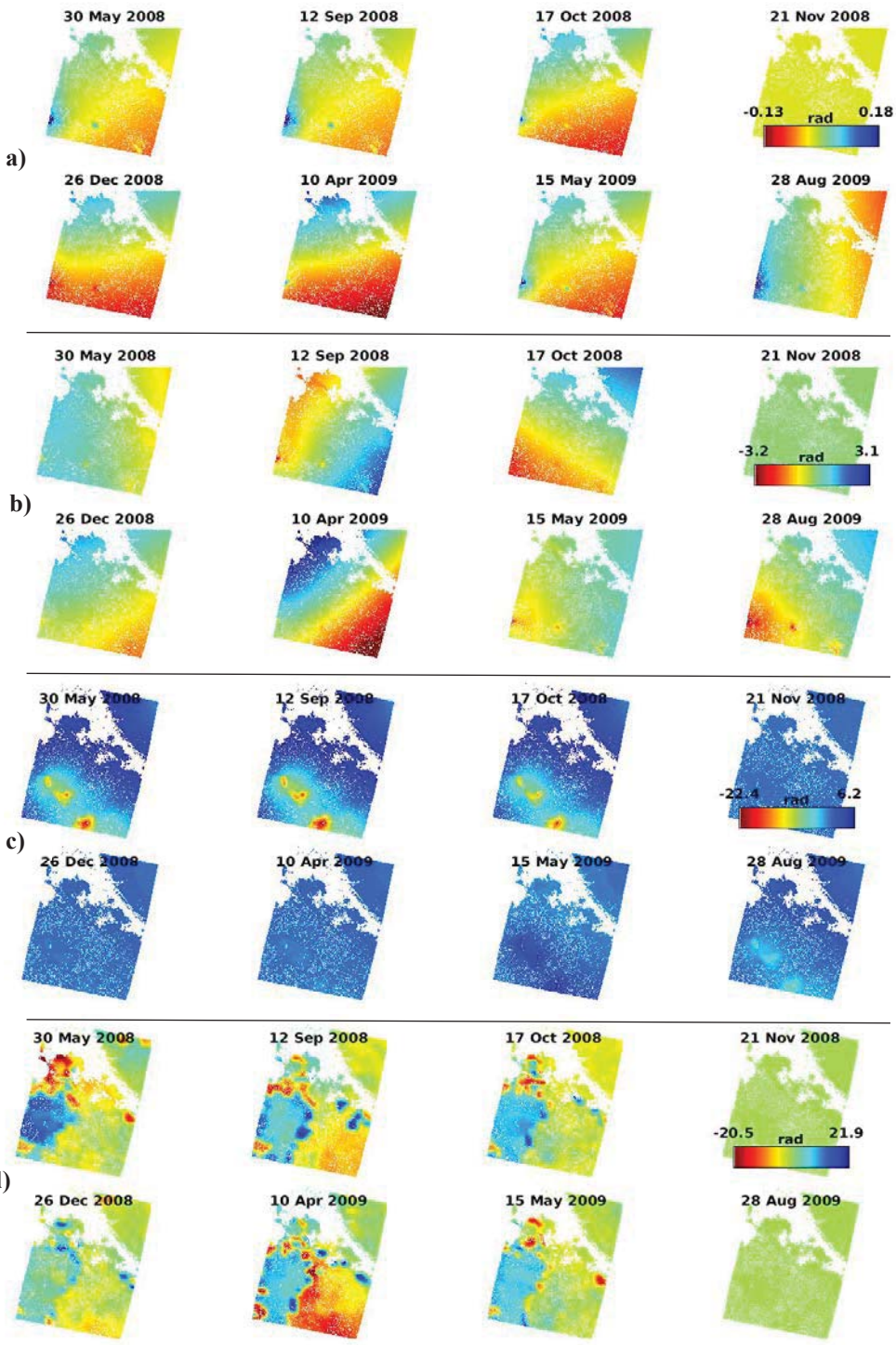

Fig. 3. Atmospheric delay in radians for diffrent correction methods and for selected images, a) empirical linear method, b) spectrometric method (wet component), c) ERA – I model (dry component), d) ERA – I model (wet component).

6 Summary

The atmospheric delay in InSAR measurements can take large values that may have a significant impact on the calculation results. Choosing the right reduction method is not easy and depends on many factors. In this case, the linear method, working well for areas with different topography, should not be used due to the impact of high displacement on the delay value. The spectrometric method seems to be the most uninfluenced, but in some cases the data are not available. The weather model, due to its low resolution, does not provide sufficiently accurate results.

The atmospheric constituent of the SAR signal is determined by various factors, that affect its value and spatial distribution, in different ways. The choice of the reduction method, should be individually selected for the particular research area and data set.

Partially processed SAR images were used in the paper in the form of single look complex (SLC) images. which have been obtained under the grant number 18310: *Identification of rock mass surface deformations on abandoned mining areas* (project manager, Wojciech Milczarek, Ph.D., Eng.), granted by the European Space Agency. The DORIS software [4] and StaMPS software [5] were used for the PSInSAR calculations. The tropospheric correction was performed using the TRAIN software [7]. The data from the European Space Agency - the spectrometric MERIS data, and the data from the European Centre for Medium-Range Weather Forecasts (ECMWF) - the ERA-I weather model, were used to determine the tropospheric delay. This work was financed by the Grant no. 0401/0128/17.

References

1. S. Dumont, Y. Klinger, A. Socquet, C. Doubre, E. Jacques, J. Struct. Geol. **95**, 48 (2017)
2. F. Barberi, J. Varet, Bull. Volcanol. **34**, 848 (1970)
3. C. Pagli, T.J. Wright, C.J. Ebinger, S-H. Yun, J.R. Cann, T. Barnie, A. Ayele, Nat. Geosci. **5**, 284 (2012)
4. B. Kampes, R, Hanssen, Z. Perski, *FRINGE* (2003)
5. A. Hooper, D. Bekaert, K. Spaans, M. Arikan, Tectonophysics **514**, 1-13 (2012)
6. R. Goldstein, Geophys. Res. Lett. **22**, 2517 (1995)
7. D.P.S. Bekaert, R.J. Walters, T.J. Wright, A.J. Hooper, D.J. Parker, Remote Sens. Environ. **170**, 40 (2015)
8. A.L. Gray, K.E. Mattar, Geophys. Res. Lett. **27**, 1451 (2000)
9. R.F. Hannsen, *Radar interferometry: Data interpretation and error analysis*, Kluwer Acad. Publ., Dordrecht (2001)
10. Z. Li, E.J. Fielding, P. Cross, R. Preusker, Int. J. Remote Sens. **30**, 3343 (2009)
11. M.-P. Doin, C. Lasserre, G. Peltzer, O. Cavalié, C. Doubre, J. Appl. Geophys. **69**, 35 (2009)
12. F. Onn, H.A. Zebker, J. Geophys. Res. **111**, 2517 (2006)
13. Y.N. Lin, M. Simons, E.A. Hetland, P. Muse, C. DiCaprio, Geochem. Geophys. Geosyst. **11** (2010)
14. Z. Li, J.-P, Muller, P. Cross, P. Albert, T. Hewison, R. Watson, J. Fisher, R. Bennartz, *MERIS User Workshop* (2003)
15. J. Saastamoinen, *Atmospheric Correction for the Troposphere and Stratosphere in Radio Ranging Satellites, in The Use of Artificial Satellites for Geodesy*, AGU, Washington, D.C. (1972)